nature geoscience

SUPPLEMENTARY INFORMATION

https://doi.org/10.1038/s41561-017-0036-x

In the format provided by the authors and unedited.

Isotopic evidence for oxygenated Mesoarchaean shallow oceans

Benjamin Eickmann[1,5]*, Axel Hofmann[1], Martin Wille[2,6], Thi Hao Bui[3], Boswell A. Wing[3,4] and Ronny Schoenberg[2]

[1]Department of Geology, University of Johannesburg, Johannesburg, South Africa. [2]Department of Geosciences, University of Tübingen, Tübingen, Germany. [3]Department of Earth and Planetary Sciences, McGill University, Montreal, QC, Canada. [4]Department of Geological Sciences, University of Colorado, Boulder, CO, USA. Present address: [5]Department of Geosciences, University of Tübingen, Tübingen, Germany. [6]Institute of Geological Sciences, University of Bern, Bern, Switzerland. *e-mail: eickmannb@gmail.com

Isotopic evidence for oxygenated Mesoarchaean oceans

Benjamin Eickmann, Axel Hofmann, Martin Wille, Thi Hao Bui, Boswell A. Wing and Ronny Schoenberg

Supplementary Material

Geological setting

The Pongola Supergroup is a Mesoarchaean volcano-sedimentary succession that was deposited ca. 3.0 – 2.9 Ga ago on continental crust of the south-eastern part of the Kaapvaal Craton (Fig. 1). Together with the Witwatersrand Supergroup, it is one of the oldest preserved cratonic cover successions. The Pongola Supergroup was deposited in a shallow-marine, epicontinental basin[1]. A two-fold subdivision of the Pongola Supergroup has been established, namely the lower volcano-sedimentary Nsuze Group and the upper, largely sedimentary Mozaan Group[2]. The supracrustal rocks were intruded by mafic and ultramafic dykes and sheets of the ca. 2.99-2.87 Ga Usushwana Complex, granite plutons as young as 2.72 Ga, and different suites of dolerite dykes and sills[3-5]. The succession has been regionally metamorphosed to lower greenschist facies, although higher metamorphic grades have been reported locally[6].

The Pongola Supergroup is exposed in a number of erosive inliers and structural remnants that extend for ca. 250 km from Amsterdam in the north to Nkandla in the south (Fig. 1) and that probably once formed part of a single sedimentary basin connected with the Witwatersrand Basin to the northwest[1]. In the study area, the White Mfolozi inlier, parts of the lower Nsuze and Mozaan groups are exposed[8]. The volcano-sedimentary succession of the Nsuze Group rests nonconformably on granitoid basement. It comprises five formations comprising subaerial basaltic to andesitic lava flows and shallow-marine sedimentary rocks (Fig. S1)[9]. The Mozaan Group unconformably overlies the Nsuze Group. It consists of a shallow-marine sedimentary succession of sandstones and shales that locally preserve abundant evidence for microbial activity in intertidal environments[10,11].

In the White Mfolozi inlier, the Nsuze Group rests on granite, different phases of which have been dated between 3.25 and 3.23 Ga using U-Pb in zircon[12]. Elsewhere, the Nsuze Group rests on granites dated at 3107 ± 4 Ma (U-Pb single zircon)[13] and contains volcanic rocks dated between 2985 ± 1 and 2968 ± 6 Ma[4,14,15]. We thus assume an age of c. 2.97 Ga for deposition of Nsuze Group sedimentary rocks.

The Chobeni Formation, focus of this study, comprises several horizons of dolostone with locally well-developed stromatolites. Based on sedimentary structures and diverse stromatolite morphologies, the dolostones have been interpreted to have formed in a shallow, tide-dominated, marine setting[16-18]. Several sedimentary units containing dolomite are present, of which the two most prominent units are referred to as the Main and Upper Carbonate sections (Fig. S1).

Samples for this study were obtained from the Upper Carbonate Section near the top of the Chobeni Formation (Fig. S1). It is c. 9 m thick, underlain by cross-bedded and very coarse-grained subtidal sandstone and overlain by shale. The section can be broadly differentiated into three units, 1) a basal unit of ripple-laminated intraclast- and quartz sand-rich dolostone deposited in a shallow subtidal environment, 2) a middle unit of oolitic/oncolitic intraclast-rich dolostone with stratiform stromatolite deposited in an intertidal to supratidal setting, and 3) an upper unit of subtidal to intertidal cross-bedded to ripple-laminated intraclast dolomitic sandstone and supratidal stratiform and massive domical microbialites. Sedimentary facies have been described in detail by ref 18. Except for recrystallization of the carbonate rocks, their textures and sedimentary structures are well preserved.

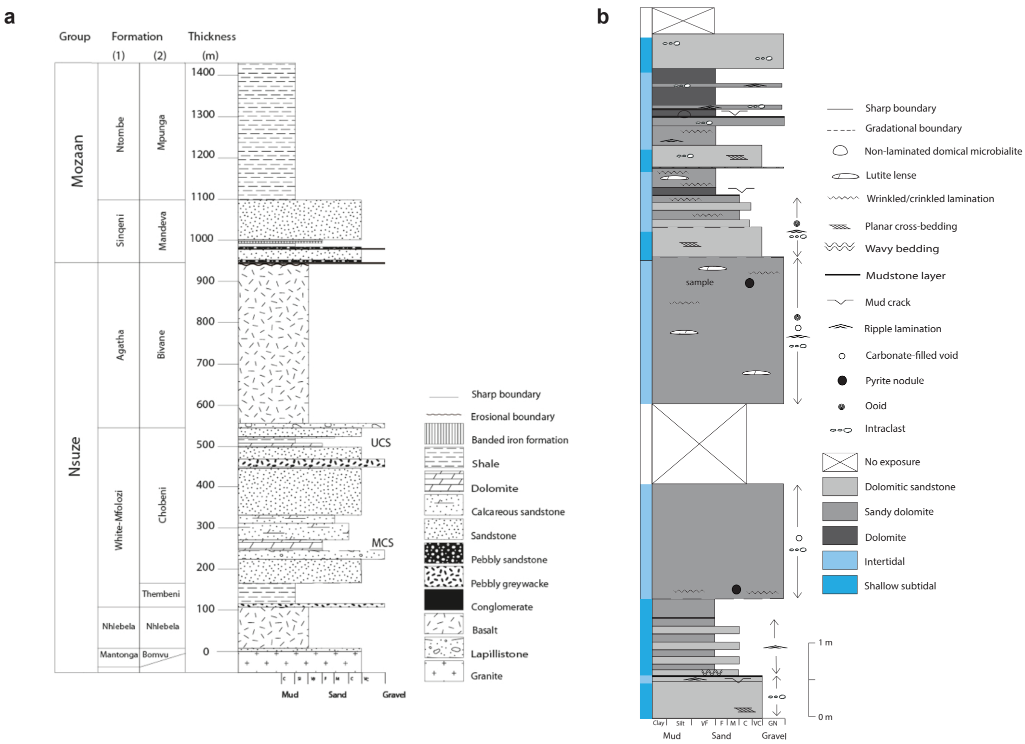

Fig. S1. **a**, Lithostratigraphic column of the Nsuze and Mozaan Groups in the White Mfolozi inlier. Formation names are after ref. 19 (column 1) and ref. 8 (column 2). MCS: Main Carbonate Section, UCS: Upper Carbonate Section (modified after ref. 7). **b**, Detailed stratigraphic column of the pyrite-bearing Upper Carbonate Section showing the stratigraphic position of the pyrite samples (modified after ref. 18).

Sample description

Pyrite nodules (Fig. S2) have only been observed in the Upper Carbonate Section. Samples for this study were obtained from surface exposure of oolitic/oncolitic intraclast-rich sandy dolostone from the central part of the section[18]. The nodules are ellipsoidal with their long axis oriented parallel to bedding. They are typically 5 to 10 mm in width, but may be as wide as 50 mm. Despite strong recrystallization, the shape of the nodules indicate formation prior to compaction. They are thus interpreted to have formed during early diagenesis. In addition to recrystallization, they are frequently brecciated by later calcite-quartz veins and are associated with secondary sulphide minerals. These include galena, sphalerite and chalcopyrite, which are only found either in or along the later calcite-quartz veins, indicating that these sulphide minerals were formed during a later-stage event after the formation of the pyrite nodules. Such a later-stage event could be linked to pulses of magmatic activity at varying temperatures. A similar formation process is inferred for carbonate-hosted Zn-Pb deposits[20]. In fact, a > 400 m thick succession of subaerial flood basalts is present 30 m above the Upper Carbonate Section (Fig. S1). Recent sulphur isotope and microbiological studies[21,22], however, suggest that sphalerite could also be of microbial origin and therefore requires low-temperature conditions. Despite recrystallization and secondary veining, the trace element geochemical signature of the carbonates reflect only minor effects of later diagenetic and metamorphic overprinting[7].

Disseminated pyrite (Fig. S3) is also present in the studied samples and typically occurs in the form of euhedral crystals (< 50 µm in size). The disseminated pyrite may have formed during diagenesis and was subsequently affected by recrystallization or it is entirely secondary. Despite a prominent clastic component in the samples in the form of abundant quartz sand grains, we found no signs of detrital pyrite.

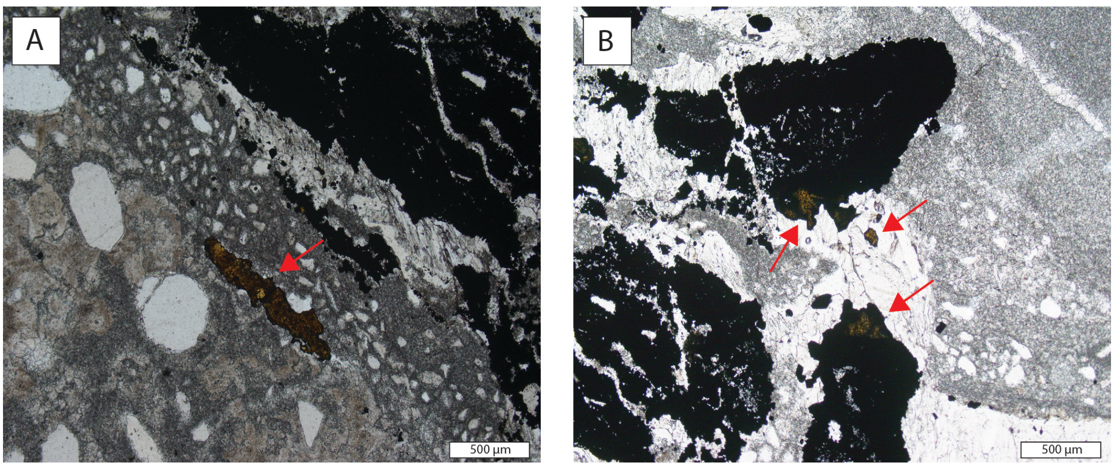

Fig. S2. Thin-section photomicrographs (A and B) of parts of pyrite nodules in plane-polarized light; pyrite appears opaque. The red arrows point to sphalerite, which is associated with later carbonate veins and the brecciation of pyrite nodules.

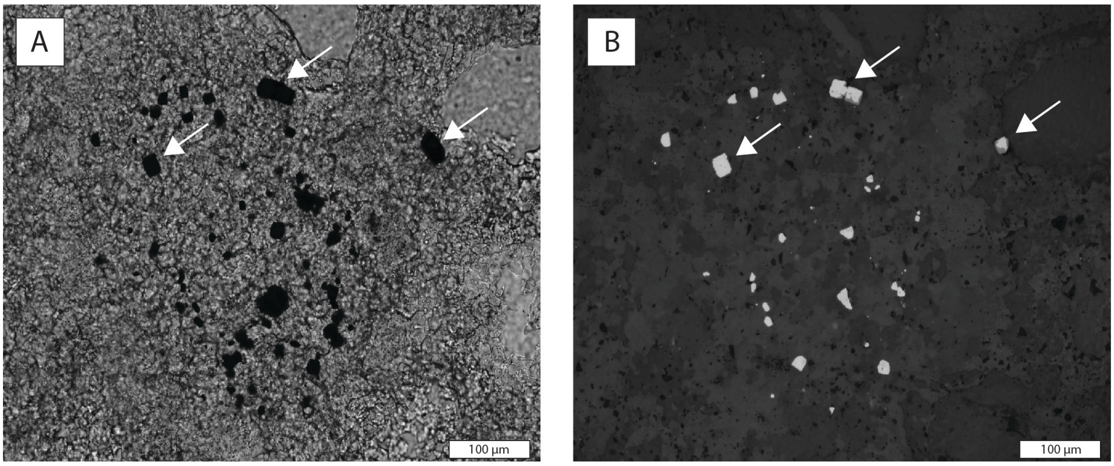

Fig. S3. Thin-section photomicrographs (A. transmitted light; B. reflected light) of representative examples of disseminated pyrite (white arrows) in dolostone of the Upper Carbonate Section.

Chemical composition of Chobeni pyrite nodules and evidence for their early diagenetic origin

Cobalt and Ni have similar ionic radii to Fe and substitute in the pyrite structure[23]. Arsenic substitutes for sulphur[24], but its chemical behaviour is more complex due to its mobility under various redox conditions. Cobalt, Ni and As, are retained at high grades of metamorphism (up to 742°C), whereas other elements (Ag, Au, Cu, Pb, Zn, Te) are lost at grades above lower greenschist facies metamorphism[25,26]. The concentrations of Co, Ni and As in sedimentary pyrites can therefore be used as reliable proxies for reconstructing the palaeoenvironmental conditions of the Chobeni Formation. Element data for the Chobeni pyrite is given in Table S4. We compared the chemical composition of pyrite from this study with sedimentary pyrites from the Witwatersrand Basin in South Africa to provide further evidence for a diagenetic origin of the Chobeni pyrites. Guy et al. (2010)[27] presented an extensive morphological and trace element study of diagenetic, detrital and epigenetic pyrites and concluded that especially the Co, Ni and As concentrations are a powerful tool for identifying different pyrite types. The Chobeni pyrites show Co and Ni concentrations similar to near-contemporaneous diagenetic pyrites from the Witwatersrand Basin and, maybe more diagnostic, almost all Chobeni pyrites plot in the light grey field of Witwatersrand diagenetic pyrite (Fig. S5), which characterizes Fe-poor host rocks (dark grey field defines Fe-rich host rocks, such banded iron formations)[27]. Although the stromatolitic carbonates in the Chobeni Formation yield maximum Fe_2O_3 concentrations of approximately 10 wt%, they can be regarded as Fe-poor host rocks[7]. In contrast to diagenetic pyrite, such as the Pongola pyrites, epigenetic Witwatersrand pyrite generally yields Co concentrations below 100 ppm[27].

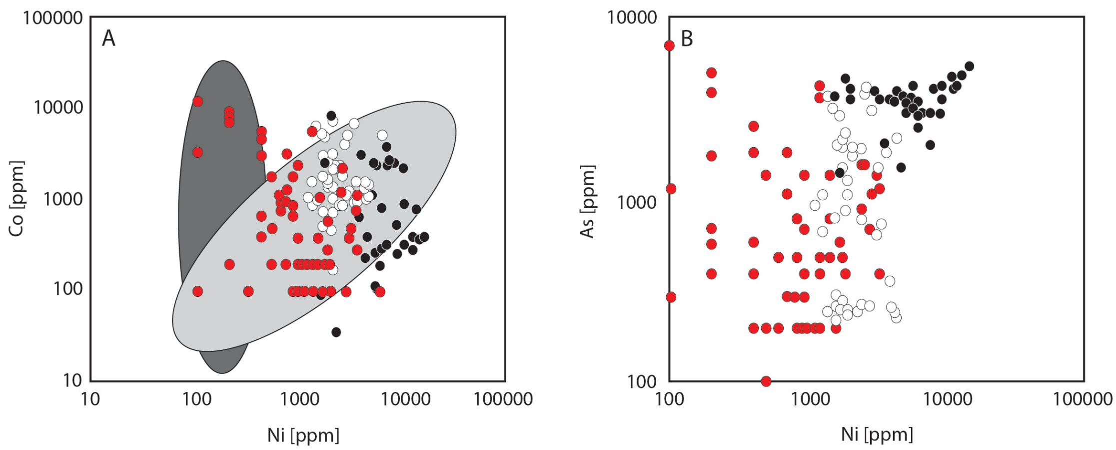

Fig. S5. Co vs Ni (a) and As vs Ni (b) plots of the Chobeni pyrite (red symbols) in comparison to diagenetic pyrite from 2.97-Gyr-old (black symbols) and 2.98-Gyr-old (white symbols) sediments of the Witwatersrand Basin. The dark grey field shows the range in Co and Ni of diagenetic pyrites from iron-rich host rocks (banded iron formations, whereas the light grey field indicates the Co and Ni variations in iron-poor hoist rocks[27].

In addition, the Chobeni pyrites do not show a positive correlation between Ni and As concentrations, which is another diagnostic feature of epigenetic pyrite[27]. All these chemical characteristics provide convincing evidence that the Chobeni pyrites are of diagenetic origin and can therefore provide information on the palaeoenvironmental conditions of this Mesoarchaean shallow-marine environment. This conclusion is further supported by detailed sedimentological and geochemical studies[7,18] of the Upper Carbonate Section, which found no textural or geochemical evidence for pervasive metamorphic overprinting. The Chobeni carbonates show rare earth element (REE) patterns that are similar to other Archaean microbialites, such as no significant cerium anomaly and a positive europium anomaly, which has been taken as evidence for precipitation from Archaean seawater[7]. Moreover, the weaker REE enrichment in the Chobeni carbonates compared to other marine Archaean carbonates is interpreted to reflect the formation in a restricted basin rather than under open ocean conditions[7]. The REE patterns even provide supporting evidence for our conclusion that continental weathering was insignificant at that time, because the europium and lanthanum anomalies in the carbonates are not correlated and this has been taken as evidence that the europium enrichment preserves a primary marine signal and was not significantly diluted by continental run-off [7].

Location of individual micro-drilled sample spots

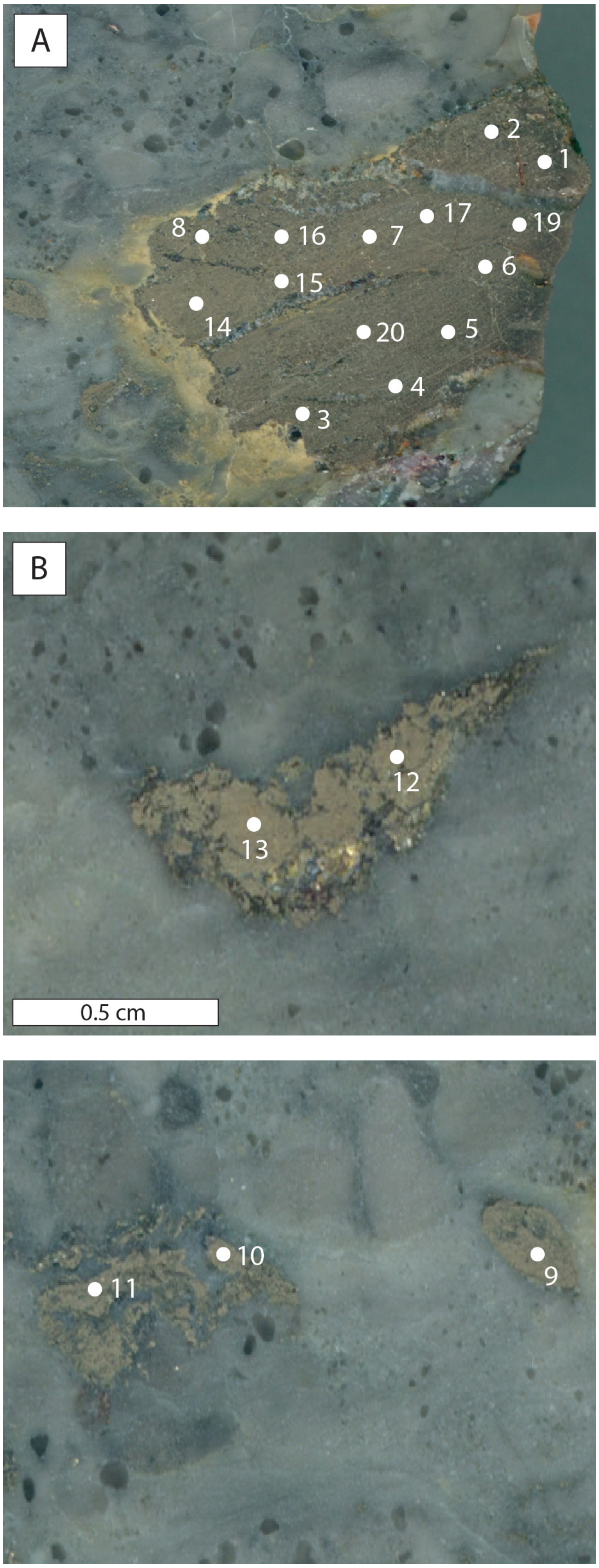

Fig. S6. Overview of individual sample spots analysed in this study.

References

1. Beukes, N.J. & Cairncross, B. A lithostratigraphic-sedimentological reference profile for the Late Archean Mozaan Group, Pongola Sequence: application to sequence stratigraphy and correlation with the Witwatersrand Supergroup. *South Afr. J. Geol.* **94**, 44-69 (1991).
2. Gold, D.J. The Pongola Supergroup. In Johnson, M.M., Anhaeuser, C.C.R. & Thomas, R.J. (Eds.) The Geology of South Africa. *Geological Society of South Africa*, 135-148 (2006).
3. Olson, J.R., Söderlund, U., Klausen, M.B. & Ernst, R.E. U-Pb baddeleyite ages linking major Archean dyke swarms to volcanic-rift forming events in the Kaapvaal Craton (South Africa), and a precise age for the Bushveld Complex. *Precambrian Res.* **183**, 490-500 (2010).
4. Mukasa, S.B., Wilson, A.H. & Young, K.R. Geochronological constraints on the magnatic and tectonic development of the Pongola Supergroup (Central Region), South Africa. *Precambrian Res*. **224**, 268-286 (2013).
5. Gumsley, A.P. *et al.,* Precise U-Pb baddeleyite age dating of the Usushwana Complex, southern Africa – Implications for the Mesoarchaean magmatic and sedimentological evolution of the Pongola Supergroup, Kaapvaal Craton. *Precambrian Res.* **267**, 174-185 (2013).
6. Hofmann, A. *et al.* The Nhlangano gneiss dome in south-west Swaziland – A record of crustal destabilization of the eastern Kaapvaal craton in the Neoarchaean. *Precambrian Res.* **258**, 109-132 (2015).
7. Bolhar, R., Hofmann, A., Siahi, M., Feng, Y.-X., Delvigne, C. A trace element and Pb isotopic investigation into the provenance and deposition of stromatolitic carbonates, ironstones and associated shales of the ~3.0 Ga Pongola Supegroup, Kaapvaal Craton. *Geochim. Cosmochim. Acta* **158**, 57-78 (2015).
8. Matthews, P.E. The pre-Karroo formations of the White Umfolozi inlier, northern Natal. *Transactions of the Geological Society of South Africa* **70**, 39-63 (1967).
9. Wilson, A.H. & Grant, E. Physical volcanology and compositions of the basaltic lava flows in the Archean Nzuse Group, White Mfolozi Inlier, South Africa. In Reimold, W.U. & Gibson, E. (Eds.) Processes on the Early Earth. Geological Society of America Special Papers, 405, 255-289 (2006).
10. Noffke, N., Beukes, N., Bower, D., Hazen, R.M. & Swift, D.J.P. An actualistic perspective into Archean worlds - (cyano-)bacterially induced sedimentary structures in the siliciclastic Nhlazatse Section, 2.9 Ga Pongola Supergoup, South Africa. *Geobiology* **6**, 5-20 (2008).
11. Hicks, N. & Hofmann, A. Stratigraphy, geochemistry and provenance of the auriferous-uraniferous, fluvial to shallow-marine Sinqeni Formation, Mozaan Group, northern KwaZulu-Natal, South Africa. *South Afr. J. Geol.* **115**, 327-344 (2012).
12. Reinhardt, J., Elburg, M.A. & Andersen, T. Zircon U-Pb age data and Hf isotopic signature of Kaapvaal basement granitiods from the Archaean White Mfolozi Inlier, Northern Kwazulu-Natal. *South Afr. J. Geol.* **118**, 473-488.
13. Kamo, S.L. & Davis, D.W. Reassessment of Archean crustal development in the Barberton Mountain Land, South Africa, based on U-Pb dating. *Tectonics* **13**, 167-192 (1994).
14. Hegner, E., Kröner, A. & Hunt, P. A precise U-Pb zircon age for the Archean Pongola Supergroup volcanics in Swaziland*. J. Afri. Earth Sci.* **18**, 339-341 (1994).
15. Nhleko, N. The Pongola Supergoup in Swaziland. PhD thesis, Rand Africaans University, Johannesburg, 299 pages.
16. Mason, T.R. & von Brunn, V. 3-Gyr-old stromatolites from South Africa. *Nature* **266**, 47-49 (1977).

17. Beukes, N.J. & Lowe, D.R. Environmental control on diverse stromatolite morphologies in the 3000 Myr Pongola Supergroup, South Africa. *Sedimentology* **36**, 383-397 (1989).
18. Siahi, M., Hofmann, A., Hegner, E. & Master, S. Sedimentology and facies analysis of Mesoarchaean stromatolitic carbonate rocks of the Pongola Supergroup, South Africa. *Precambrian Res*. **278**, 244-263 (2016).
19. Joubert, P. & Johnson, M.R. Abridged lexicon of South Africa Stratigraphy. South African Committee for Stratigraphy, Council for Geoscience, 160 pages (1998).
20. Pašava, J, Torres, F. & Chrastny, V. Zinc and sulphur isotope variations in sphalerite from carbonate-hosted zinc deposits, Cantabria, Spain. *Miner. Deposita* **49**, 797-807 (2014).
21. Labrenz, M. et al. Formation of sphalerite (ZnS) deposits in natural biofilms of sulphate-reducing bacteria. *Science* **290**, 1744-1747 (2000).
22. Kucha, H., Schroll, E., Raith, J. G., & Halas, S. Microbial sphalerite formation in carbonate-hosted ZN-Pb ores, Bleiberg, Austria: Micro- to nanotextural and sulphur isotope evidence. *Econ. Geol.* **105**, 1005-1023 (2020).
23. Huston, D. L. *et al.* Trace elements in sulfide minerals from Eastern Australian volcanic-hosted massive sulphide deposits: Part I. Proton microprobe analyses of pyrite, chalcopyrite, and sphalerite; Part II. Selenium levels in pyrite: comparison with $\delta^{34}S$ values and implications for the source of sulfur in volcanogenic hydrothermal systems. *Econ. Geol.* **90**, 1167-1196 (1995).
24. Lowers, H. A. *et al.* Arsenic incorporation into authigenic pyrite, Bengal Basin sediment, Bangladesh. *Geochim. Cosmochim. Acta* **71**, 2699-2717.
25. Vaughan, D. J. & Rosso, K. L. Chenical bonding in sulfide minerals. *Rev. Min. and Geochem*. **61**, 231-264 (2006).
26. Large, R. R. *et al.* Multi-stage sedimentary and metamorphic origin of pyrite and gold in the Giant Sukhoi Log deposit, Lena Goldfield, Russia. *Econ. Geol.* **102**, 1233-1267 (2007).
27. Guy, B. M., Beukes, N. J. & Gutzmer, J. Paleoenvironmental controls on the texture and chemical composition of pyrite from non-conglomeratic sedimentary rocks of the Mesoarchean Witwatersrand Supergroup, South Africa. *South Afr. J. Geol.* **113,** 195-228.

Table S1. Multiple sulphur and iron isotope data of sedimentary pyrites from the Chobeni Formation, Pongola Supergroup, South Africa. The uncertainty (2 s.d.) for individual iron isotope measurement is 0.05‰.

Sample ID	$\delta^{34}S$	$\Delta^{33}S$	$\Delta^{36}S$	$\delta^{56}Fe$
Nodule pyrite				
NCD4-1	-17.6	-0.784	1.08	n.a.
NCD4-2	-9.6	-0.644	0.98	-1.27
NCD4-3	-4.8	-0.359	0.63	n.a.
NCD4-4	-3.9	-0.327	0.60	-1.04
NCD4-5	-6.2	-0.516	0.73	-1.11
NCD4-6	-11.1	-0.859	1.92	-1.29
NCD4-7	-7.8	-0.583	1.34	-1.26
NCD4-8	-9.2	-0.507	0.87	-1.16
NCD4-10	-4.6	-0.307	0.63	n.a.
NCD4-11	-6.3	-0.425	1.02	-1.08
NCD4-12	-22.4	-0.887	1.34	n.a.
NCD4-13	-21.8	-0.621	1.82	-0.88
NCD4-14	-0.5	-0.383	0.50	-1.23
NCD4-15	-1.9	-0.388	0.62	-1.13
NCD4-16	-5.8	-0.623	0.96	-1.13
NCD4-17	-11.5	-0.927	1.09	-1.31
NCD4-18	-4.5	-0.486	1.15	-1.09
NCD4-19	-19.2	-0.902	1.29	-1.15
NCD4-20	n.a.	n.a.	n.a.	-1.11
Disseminated pyrite in stromatolitic dolostone				
NCD4-11A	-6.9	-0.503	0.86	n.a.
NCD4-12A	-7.6	-0.471	0.82	n.a.
NCD4-13A	-5.9	-0.490	0.82	n.a.
NCD4-14A	-7.2	-0.519	0.80	n.a.
NCD4-15A	-7.1	-0.522	0.83	n.a.

n.a.: not analysed.

Table S2. Multiple sulphur isotope literature data of Archaean sedimentary pyrites as shown in Fig. 2.

Sample ID	$\delta^{34}S$	$\Delta^{33}S$	$\Delta^{36}S$
Shen et al. 2009			
YS-NP124-new extraction	-7.8	-0.582	-0.87
NP-124-sample from S01	-3.3	0.022	-1.27
YS-NP-89-new extraction	-19.7	-1.213	0.49
NP-89-sample from S01	-16.1	-1.183	
GIS 95.0 II macroscopic	-1.3	-0.215	-0.15
GIS 96.6 II microscopic	-1.8	-0.290	-0.26
GIS 96.7 II microscopic	-4.7	-0.333	0.26
NP21019A-Py	-4.7	-0.467	0.16
NP21019B-Py	-6.3	-0.495	0.52
NP21019C-Py	-5.6	-0.418	0.39
NP21021-Py	-8.5	-0.652	0.40
NP21022A-Py	-10.4	-0.805	0.93
NP21025-Py	-8.1	-0.667	0.45
NP21026-Py	-9.6	-0.671	0.01
NP21031-Py	-7.2	-0.699	0.62
NP21016-Py	-12.9	-0.829	
NP21029-Py	-10.3	-1.269	1.31
Zhelezinksaia et al. 2014			
GDR-1272p9@1	-10.25	-1.63	1.71
GDR-1272p9@2	-6.64	-1.51	1.84
GDR-1272p9@3	-2.86	-1.18	0.98
GDR-1272p9@4	-5.52	-1.35	1.17
GDR-1272p9@5	-10.27	-1.59	1.08
GDR-1272p9@6	-10.98	-1.7	1.25
GDR-1272p9@7	-10.18	-1.68	1.31
GDR-1272p9@8	-1.05	-1.92	2.02
GDR-1272p9@9	0.1	-2.1	2.51
GDR-1272p9@10	-8.63	-1.57	1.38
GDR-1272p9@11	-9.79	-1.53	1.55
GDR-1272p9@12	-10.24	-1.62	1.69
GDR-1272p9@13	-2.77	-1.92	2.68
GDR-1272p9@14	-10.62	-1.65	1.78
GDR-1272p9@15	-10.24	-1.66	1.54
GDR-1272p9@16	-0.39	-2.05	2.55
GDR-1272p9@17	-0.91	-2.15	2.71
GDR-1272p9@18	-8.62	-1.44	1.67
GDR-1272p9@19	-10.3	-1.6	1.85
GDR-1272p9@20	-8.69	-1.74	2.14
GDR-1261P1@1	-8.65	-1.86	2.02
GDR-1261P1@2	-11.27	-1.89	1.87
GDR-1261P1@3	-1.56	-0.22	0.8
GDR-1261P1@4	-3.44	-1.87	2.32
GDR-1261P1@5	-10.26	-2.01	1.7
GDR-1261P1@6	-9.93	-1.91	2.11

GDR-1261P1@7	1.58	-2.05	2.77
GDR-1261P1@8	-11.51	-2.05	2.25
GDR-1261P1@9	-6.89	-1.98	2.05
GDR-1261P1@10	-1.44	-1.98	1.98
GDR-1261P1@11	-3.71	-1.51	1.7
GDR-1261P1@12	-6.83	-2.01	1.67
GDR-1261P1@13	-9.32	-1.98	1.58
GDR-1261P1@14	-29.96	-1.98	1.85
GDR-1261P1@15	-13.46	-1.58	1.11
GDR-1261P1@16	-5.9	-2.02	1.82
GDR-1261P1@17	-10.06	-1.98	1.98
GDR-1261P1@18	-2.23	-1.82	1.82
GDR-1266p72_1@1	-38.37	-1.97	2
GDR-1266p72_1@2	-33.91	-1.9	1.77
GDR-1266p72_1@3	-12.05	-0.74	1.14
GDR-1266p72_1@4	-34.09	-1.95	2.01
GDR-1266p72_1@5	-31.29	-1.97	2.23
GDR-1266p72_1@6	-29.87	-1.44	1.68
GDR-1266p72_1@7	-26.47	-2.01	2.33
GDR-1308p00@1	-18.16	-3.11	2.48
GDR-1308p08@2	-18.08	-3.11	2.74
GDR-1308p08@3	-17.52	-3.02	2.37
GDR-1308p08@4	-16.88	-2.93	1.34
GDR-1308p08@5	-19.32	-3.15	2.91
GDR-1272p2-1@1	-8.1	-1.44	1.55
GDR-1272p2-1@2	-9.09	-1.34	1.63
GDR-1272p2-1@3	-4.75	-1.23	2
GDR-1272p2-1@4	1.1	-1.14	1.92
GDR-1272p2-1@5	-9.33	-1.32	2.05
GDR-1272p2-2@1	-8.45	-1.55	1.61
GDR-1272p2-2@2	-7.27	-1.63	1.99
GDR-1272p2-2@3	-6.48	-1.5	1.5
GDR-1272p2-2@4	1.02	-1.76	1.93
GDR-1272p2-2@5	-7.2	-1.55	1.76
GDR-1272p2-2@6	-0.66	-1.98	1.81
GDR-1272p2-2@7	-6.33	-1.54	1.4
GDR-1272p2-2@8	-6.96	-1.52	1.34
GDR-1272p2-2@9	-5.06	-0.01	0.17
GDR-1272p2-2@10	-6.57	-1.65	1.45
GDR-1272p2-2@11	-5.57	-1.72	1.54
GDR-1272p2-2@12	-6.89	-1.62	1.41
GDR-1266p72@1	-15.11	-1.1	1.51
GDR-1266p72@2	-19.67	-1.33	1.58
GDR-1266p72@3	-36.14	-1.89	1.83
GDR-1266p72@4	-35.23	-1.91	1.85
GDR-1266p72@5	-36.82	-1.96	1.96
GDR-1266p72@6	-33.4	-1.96	1.3
GDR-1266p72@7	-21.32	-1.39	1.15
GDR-1266p72@8	-34.88	-1.98	0.98

Partridge et al. 2008

Wittenoom Formation (2565 ± 9 Ma)			
UQ4	-8.15	-1.04	n.a.
UQ4	-8.87	-0.85	n.a.
UQ4	-8.45	-0.82	n.a.
UQ4	-8.28	-0.92	n.a.
UQ4	-7.16	-0.79	n.a.
UQ4	-7.89	-0.69	n.a.
UQ4	-11.5	-1.15	n.a.
UQ4	-12.23	-1.2	n.a.

Farquhar et al. 2013

GKF01_mount4_1102_grain-1@1	-18.83	-0.83	1.89
GKF01_mount4_1102_grain-1@2	-20.13	-0.97	2.13
GKF01_mount4_1102_grain-1@3	-20.61	-0.96	1.86
GKF01_mount4_1102_grain-1@4	-13.31	-0.22	1.06
GKF01_mount4_1102_grain-1@5	-16.04	-0.54	1.27
GKF01_mount4_1102_grain-1@6	-19.02	-0.82	1.91
GKF01_mount4_1102_grain-1@7	-20.35	-0.81	1.79
GKF01_mount4_1102_grain-1@8	-20.79	-0.81	1.49
GKF01_mount4_1102_grain-1@9	-18.94	-0.86	2.14
GKF01_mount4_1102_grain-1@10	-19.68	-0.87	1.71
GKF01_mount4_1102_grain-1@11	-20.86	-0.9	1.61
GKF01_mount4_1102_grain-1@12	-20.64	-0.87	1.52
GKF01_mount4_1102_grain-1@13	-19.69	-0.84	1.93
GKF01_mount4_1102_grain-1@14	-20.02	-0.82	1.56
GKF01_mount4_1102_grain-1@15	-19.79	-0.91	1.81
GKF01_mount4_1102_grain-1@16	-19.88	-0.89	2.03
GKF01_mount4_1102_grain-1@17	-17.27	-0.62	1.34
GKF01_mount4_1102_grain-1@18	-19.04	-0.78	1.68
GKF01_mount4_1102_grain-1@19	-20.1	-0.91	1.92
GKF01_mount4_1102_grain-1@20	-21.55	-0.92	1.81
GKF01_mount4_1102_grain-1@21	-19.01	-0.89	1.97
GKF01_mount4_1102_grain-1@22	-18.32	-0.94	2
GKF01_mount4_1102_grain-1@23	-20.8	-0.91	1.85
GKF01_mount4_1102_grain-1@24	-19.71	-0.85	1.55
GKF01_mount4_1102_grain-1@25	-18.55	-0.81	1.58
GKF01_mount4_1102_grain-1@26	-20.38	-0.85	1.94
GKF01_mount4_1102_grain-1@27	-16.2	-0.62	1.62
GKF01_mount4_1102_grain-1@28	-19.62	-0.87	1.85
GKF01_mount4_1102_grain-1@29	-19.78	-0.87	1.85
GKF01_mount4_1102_grain-1@30	-19.82	-0.85	1.46
GKF01_mount4_1102_grain-1@31	-15.12	-0.58	1.44
GKF01_mount4_1102_grain-1@32	-17.1	-0.73	1.4
GKF01_mount4_1102_grain-1@33	-20.17	-0.88	1.52
GKF01_mount4_1102_grain-1@34	-20.63	-0.9	1.74
GKF01_mount4_1102_grain-1@35	-19.29	-0.83	1.92
GKF01_mount4_1102_grain-1@36	-19.34	-0.78	1.74
GKF01_mount4_1102_grain-1@37	-20.75	-0.85	1.89
GKF01_mount4_1102_grain-1@38	-18.09	-0.73	1.8

GKF01_mount4_1102_grain-1@39	-17.9	-0.62	1.68
GKF01_mount4_1102_grain-1@40	-14.18	-0.33	0.56
GKF01_mount4_1102_grain-1@41	-20.45	-0.88	1.97
GKF01_mount4_1102_grain-1@42	-19.97	-0.9	2.2
GKF01_mount4_1102_grain-1@43	-15.36	-0.62	1.42
GKF01_mount4_1102_grain-1@44	-13.34	-0.39	1.28
GKF01_mount4_1102_grain-1@45	-20.5	-0.87	1.91
GKF01_mount4_1102_grain-1@46	-20.28	-0.85	1.79
GKF01_mount4_1102_grain-1@47	-20.48	-0.85	1.8
GKF01_mount4_1102_grain-1@48	-19.46	-0.96	2.02
GKF01_mount4_1102_grain-1@49	-20.41	-0.75	1.98
GKF01_mount4_1102_grain-1@50	-20.39	-0.65	1.49
GKF01_mount4_1102_grain-1@51	-19.91	-0.8	1.84
GKF01_mount4_1102_grain-1@52	-19.53	-0.86	1.85
GKF01_mount4_1102_grain-1@53	-20.32	-0.93	1.78
GKF01_mount4_1102_grain-1@54	-20.16	-0.78	1.75
GKF01_mount4_1102_grain-1@55	-18.33	-0.78	1.6
GKF01_mount4_1102_grain-1@56	-19.93	-0.76	1.86
GKF01_mount4_1102_grain-1@57	-19.71	-0.68	1.62
GKF01_mount4_1102_grain-1@58	-20.39	-0.8	1.85
GKF01_mount4_1102_grain-1@59	-19.55	-0.8	1.85
GKF01_mount4_1102_grain-1@60	-19.54	-0.6	1.76
GKF01_mount4_1102_grain-1@61	-20.26	-0.8	1.63
GKF01_mount4_1102_grain-1@62	-17.67	-0.69	1.82
GKF01_mount4_1102_grain-1@63	-20.4	-0.81	1.96
GKF01_mount4_1102_grain-1@64	-18.5	-0.69	1.56
GKF01_mount4_1102_grain-1@65	-18.53	-0.71	1.1
GKF01_mount4_1102_grain-1@66	-19.06	-0.79	1.27
GKF01_mount4_1102_grain-1@67	-16.42	-0.67	1.44
GKF01_mount4_1102_grain-1@68	-20.34	-0.8	1.89
GKF01_mount4_1102_grain-1@69	-19.53	-0.68	1.72
GKF01_mount4_1102_grain-1@70	-19.25	-0.57	1.78
GKF01_mount4_1102_grain-1@71	-19.07	-0.81	1.91
GKF01_mount4_1102_grain-1@72	-20.65	-0.93	2.05
GKF01_mount4_1102_grain-1@73	-18.71	-0.72	1.6

Table S3. Literature iron isotope data of Archaean sedimentary pyrites as shown in Fig. 3.

Sample ID	$\delta^{34}S$	$\delta^{56}Fe$
Hofmann et al. 2009		
Pongola Supergroup, Mozaan Contact Reef, Denny Dalton Mine		
PO/DD1-A	0.5	-0.56
PO/DD1-B	0.4	-0.52
PO/DD1-C	2.6	-0.56
PO/DD1-D	2.9	-0.51
PO/DD1-F	0.7	-0.81
PO/DD1-G	0.3	-0.63
PO/DD2-A	0.7	-0.61
PO/DD2-C	0.2	-0.72
Dominion Reef, Dominion Reefs Uranium Mine		
DR-1	2.1	-0.17
Rounded pyrite, Cheshire Formation, Belingwe Greenstone Belt, Zimbabwe		
B/E1-B	-6.1	-3.59
B/E1-C1	-6.4	-2.76
B-E1-D1	-9.3	-2.49
B-E1-E	-12.8	-1.76
B/E1-F1	-8.1	-2.89
B/E1-G1	-9.5	-2.80
Jimmy Member, Manjeri Formation, Belingwe Greenstone Belt, Zimbabwe, NERCMAR core		
D1	-6.6	-2.16
D2	-2.3	-1.84
D4	-8.5	-2.69
D5	-10.0	-2.42
D6A	-6.5	-2.30
D6B	-5.4	-1.87
Marin-Carbonne et al. 2014		
Nodule 1		
AH-sample9-pt@1	3.9	0.45
AH-sample9-pt@02	4.81	-0.1
AH-sample9-pt@03	3.41	-1.19
AH-sample9-pt@04	3.1	-0.19
AH-sample9-pt@05	2.58	-1.6
AH-sample9-pt@06	2.05	-1.95
AH-sample9-pt@07	-0.55	-2.11
AH-sample9-pt@08	2.91	-1.92
AH-sample9-pt@10	4.83	-1.99
AH-sample9-pt@11	4.11	-1.39
AH-sample9-pt@12	3.92	-1.92

AH-sample9-pt@13	4.31	-1.76
AH-sample9-pt@14	2.43	-1.79
AH-sample9-pt@15	2.98	-1.53
AH-sample9-pt@16	1.98	-1.36
AH-sample9-pt@17	0.83	-1.16
AH-sample9-pt@18	2.2	-1.17
AH-sample9-pt@19	0.64	-0.25
AH-sample9-pt@20	2.94	-0.14
AH-sample9-pt@21	3.84	-0.67
AH-sample9-pt@23	2.96	-0.29
Nodule 2		
sample9pt@1	2.26	-0.11
sample9pt@03	2.39	-0.27
sample9pt@04	4.85	0.75
sample9pt@06	7.76	-0.73
sample9pt@08	0.73	-0.42
sample9pt@10	4.02	-0.38
sample9pt@13	1.3	-1.08
sample9pt@14	0.94	-1.58
sample9pt@15	1.92	-1.53
sample9pt@16	2.25	-0.79
sample9pt@17	0.56	-0.3
sample9pt@18	1.5	-0.45
sample9pt@19	0.36	-0.01

Table S4. Electron microprobe data of the Chobeni pyrite.

Sample ID	S [wt%]	Mn [wt%]	Fe [wt%]	Co [wt%]	Ni [wt%]	Cu [wt%]	Zn [wt%]	As [wt%]	Se [wt%]	Pb [wt%]	Total
NCD4-1_12_01	52.35	0	45.95	0.19	0.05	0	0.02	0.14	0	0	98.70
NCD4-1_12_02	53.74	0	46.35	0.01	0.03	0	0	0	0	0	100.13
NCD4-1_12_03	52.6	0	45.32	0.07	0.08	0.01	0.03	0.08	0.02	0.21	98.41
NCD4-1_12_021	53.45	0	46.09	0.1	0.06	0	0.29	0.05	0	0.04	100.08
NCD4-1_12_025	53.48	0	46.25	0.03	0	0	0.02	0.03	0	0.07	99.87
NCD4-1_12_026	53.3	0	45.98	0.6	0.04	0.01	0.06	0.19	0	0.01	100.18
NCD4-1_12_027	53.42	0	45.71	0.57	0	0	0.03	0.31	0	0	100.04
NCD4-1_12_030	52.9	0	45.8	0.04	0.09	0	0	0.07	0	0.03	98.92
NCD4_1 06 013	53.32	0	45.89	0.01	0.25	0	0.07	0.16	0	0.04	99.74
NCD4_1 06 017	53.41	0.01	46.19	0.02	0.05	0	0.06	0.01	0	0.07	99.83
NCD4_1 06 018	52.96	0.01	45.79	0.01	0.53	0	0.01	0	0.02	0	99.33
NCD4_1 06 019	53.5	0.01	45.72	0	0.4	0	0.01	0	0	0	99.65
NCD4_1 06 038	53.66	0.01	45.98	0.36	0.01	0.09	0.02	0.12	0	0.01	100.26
NCD4_1 06 039	53.36	0	45.95	0.1	0.07	0.04	0.04	0.11	0	0	99.67
NCD4_1 06 041	53.83	0.01	46.23	0.57	0	0	0.02	0.09	0	0	100.76
NCD4_1 06 042	53.18	0	45.33	1.03	0	0	0	0.57	0	0	100.12
NCD4_1 06 044	53.95	0	46.16	0.01	0.12	0	0.01	0.02	0.02	0	100.28
NCD4_1 06 045	54.39	0	46.4	0.02	0.05	0	0.03	0	0	0.01	100.91
NCD4_1 06 046	53.86	0	45.83	0.33	0.04	0	0	0.06	0	0.01	100.13
NCD4_1 06 047	53.66	0.01	46.48	0	0.12	0	0.01	0.02	0.01	0	100.31
NCD4_1 06 048	54.03	0	46.31	0.08	0.06	0	0	0.05	0	0	100.53
NCD4_1 06 049	53.73	0	46.12	0.01	0.08	0.02	0	0.02	0.01	0.02	100.01
NCD4_1 06 050	53.49	0.01	46.6	0.01	0.09	0	0.01	0.02	0.01	0.02	100.26
NCD4_1 06 051	53.4	0.01	46.22	0.34	0.07	0	0.03	0.19	0	0	100.28
NCD4_1 06 052	53.2	0	45.28	0.9	0	0	0.02	0.38	0	0	99.78
NCD4_1 06 053	53.58	0	46.66	0	0.09	0	0.04	0	0	0	100.37
NCD4_1 06 054	54.08	0	45.81	0.77	0.02	0	0.05	0.18	0.02	0.02	100.96
NCD4_1 06 055	52.99	0	46.04	0.02	0.12	0	0.19	0.43	0.01	0.01	99.81
NCD4_1 06 066	53.38	0.01	45.89	0.85	0.02	0	0.17	0.41	0.02	0	100.76
NCD4_1 06 068	53.54	0	46.51	0.01	0.1	0.01	0.04	0.02	0.01	0	100.24
NCD4_1 06 069	53.87	0	46.24	0.02	0.1	0	0	0	0	0	100.24
NCD4_1 06 070	53.23	0	45.63	0.12	0.32	0	0.01	0.12	0.01	0.22	99.66
NCD4_1 06 071	52.97	0	45.73	0.03	0.17	0	0.01	0.05	0.01	0.42	99.37
NCD4_1 06 072	52.82	0	45.59	0.02	0.16	0	0	0.06	0	0.33	98.98
NCD4_1 06 073	53.26	0.01	46.6	0.07	0.04	0.01	0	0.02	0	0.06	100.06
NCD4_1 06 074	53.65	0.01	46.19	0.02	0.07	0	0.02	0	0	0	99.96
NCD4_1 06 078	53.95	0	45.34	0.89	0.02	0.02	0.22	0.52	0.01	0.05	101.01
NCD4_1 06 079	53.54	0	45.59	0.06	0.17	0.01	0.17	0.15	0	0.22	99.91
NCD4_1 06 080	52.78	0	45.81	0.02	0.14	0	0.02	0.05	0	0.14	98.97
NCD4_1 06 081	53.05	0	46.3	0.04	0.04	0	0	0.04	0.01	0.01	99.51
NCD4_1 06 082	53	0.01	46.22	0.09	0.08	0	0.02	0.03	0	0	99.46
NCD4_1 06 083	53.33	0	45.93	0.11	0.14	0	0.29	0.08	0	0.03	99.92
NCD4_1 06 084	53.14	0	45.22	1.26	0.01	0	0.02	0.74	0	0	100.39
NCD4_1 06 085	53.84	0	45.95	0.5	0.04	0	0.02	0.26	0	0	100.61
NCD4_1 06 086	53.65	0	46.11	0.25	0.09	0	0.03	0.14	0	0.05	100.32
NCD4_1 06 087	53.48	0	45.89	0.24	0.23	0	0.02	0.16	0.01	0.09	100.12
NCD4_1 06 088	53.03	0	46.34	0.17	0.12	0	0	0.04	0	0	99.70
NCD4_1 06 089	53.52	0	46.01	0.02	0.18	0	0.01	0.04	0	0.14	99.92
NCD4_1 06 090	53.41	0	46	0.04	0.14	0.01	0	0.14	0.01	0.12	99.87

Sample ID	S [wt%]	Mn [wt%]	Fe [wt%]	Co [wt%]	Ni [wt%]	Cu [wt%]	Zn [wt%]	As [wt%]	Se [wt%]	Pb [wt%]	Total
NCD4_1 06 091	53.26	0.01	46.15	0.01	0.12	0	0.02	0	0.01	0.02	99.60
NCD4_1 06 092	53.45	0	46.1	0.01	0.15	0.02	0	0.02	0	0.04	99.80
NCD4_1 06 093	53.07	0	46.49	0.02	0.1	0	0	0.02	0	0.05	99.75
NCD4_1 06 094	53.97	0.01	46.44	0.13	0.23	0	0.01	0.09	0.01	0	100.89
NCD4_1 06 095	52.98	0	46.34	0.14	0.07	0.02	0	0.03	0.02	0	99.60
NCD4_1 06 096	53.52	0	45.98	0.03	0.32	0	0	0.04	0	0.06	99.95
NCD4_1 06 097	53.39	0	46.4	0.05	0.05	0	0	0.02	0	0.02	99.93
NCD4_1 06 098	53.25	0	45.87	0.08	0.31	0	0.01	0.14	0.01	0.08	99.75
NCD4_1 06 099	53.36	0	46.35	0.02	0.02	0	0	0.07	0	0	99.84
NCD4_1 06 0100	53.33	0	46.35	0.12	0.06	0.01	0	0.02	0	0	99.90
NCD4_1 06 0101	52.83	0	45.4	1	0.02	0	0.01	0.52	0	0	99.77
NCD4_1 06 0102	53.62	0	45.65	0.61	0.12	0	0.02	0.38	0.01	0.01	100.42
NCD4_1 06 0103	54.39	0	46.14	0.19	0.08	0	0	0.05	0	0	100.84
NCD4_1 06 0104	53.23	0	46.37	0.05	0.05	0.01	0	0.02	0	0	99.73
NCD4_1 06 0105	53.35	0	45.69	0.04	0.27	0.03	0	0.07	0	0.14	99.59
NCD4_1 06 0106	53.38	0	45.92	0.02	0.09	0	0	0.04	0	0.2	99.66
NCD4_1 06 0107	53.02	0.01	46.13	0.05	0.28	0	0	0.11	0	0.06	99.65
NCD4_1 06 0108	53.03	0.01	45.66	0.02	0.12	0.01	0	0.05	0	0.12	99.03
NCD4_1 06 0109	53.05	0	46.36	0.01	0.01	0	0	0.03	0	0.04	99.50
NCD4_1 06 0110	53.84	0	46.32	0.02	0.11	0	0	0.02	0.02	0	100.33
NCD4_1 06 0111	53.67	0	46.47	0	0.02	0	0	0.04	0	0.07	100.26
NCD4_1 06 0112	53	0	45.74	0.01	0.18	0	0	0.04	0	0.25	99.20
NCD4_1 06 0113	53.28	0	45.84	0.59	0	0	0	0.1	0.02	0.02	99.86
NCD4_1 06 0114	53.18	0	46.28	0	0.09	0	0.03	0.03	0	0	99.62
NCD4_1 06 0115	53.37	0	46.35	0	0.02	0	0	0.06	0.02	0.04	99.86